Inclusive Δ^{++} production in $\pi^- p$ interactions at 147 GeV/c

D. Brick, D. Fong,* M. Heller,† A. M. Shapiro, and M. Widgoff
Brown University, Providence, Rhode Island 02912

F. Bruyant
CERN, Geneva 23, Switzerland

D. Bogert and M. Johnson
Fermilab, Batavia, Illinois 60510

R. Burnstein, C. Fu,‡ D. Petersen,§ M. Robertson,‖ and H. Rubin
Illinois Institute of Technology, Chicago, Illinois 60616

R. Sard, A. Snyder,¶ and J. Tortora**
University of Illinois, Urbana, Illinois 61801

E. D. Alyea, Jr.
Indiana University, Bloomington, Indiana 47401

C.-Y. Chien, P. Lucas,†† A. Pevsner, and R. Zdanis
Johns Hopkins University, Baltimore, Maryland 21218

F. Barreiro, O. Benary,‡‡ J. E. Brau,§§ J. Grunhaus,‖‖ E. S. Hafen, R. I. Hulsizer, U. Karshon,¶¶ V. Kistiakowsky, A. Levy,‖‖ A. Napier, I. A. Pless, J. P. Silverman, P. C. Trepagnier, J. Wolfson,*** and R. K. Yamamoto
Massachusetts Institute of Technology, Cambridge, Massachusetts 02139

H. Cohn
Oak Ridge National Laboratory, Oak Ridge, Tennessee 37830

R. F. Jacques, T. C. Ou, R. J. Plano, and T. L. Watts
Rutgers University, New Brunswick, New Jersey 08903

E. B. Brucker, E. L. Koller, P. Stamer, and S. Taylor
Stevens Institute of Technology, Hoboken, New Jersey 07030

W. Bugg, G. Condo, T. Handler, and E. Hart
University of Tennessee, Knoxville, Tennessee 37916

H. Kraybill, D. Ljung, T. Ludlam, and H. D. Taft
Yale University, New Haven, Connecticut 06520

(Received 30 June 1977; revised manuscript received 22 June 1978)

The inclusive production of the $\Delta^{++}(1232)$ resonance in $\pi^- p$ collisions at 147 GeV/c has been studied. The Δ^{++} is found to be produced in comparable amounts in four-, six-, eight-, and ten-prong events. The Feynman-x, t', P_T^2, and the decay angular distributions of the Δ^{++} are found to be consistent with the predictions of a one-pion-exchange model with absorption. Essentially all of the Δ^{++} are found to be associated with a $\Delta^{++}\pi^-$ low-mass enhancement. The Δ^{++} cross section is approximately constant from 11 to 205 GeV/c, which could indicate that the Δ^{++} is a decay product of a target-fragmentation object. While the one-pion-exchange character of the Δ^{++} production and the target-fragmentation character of the $\Delta^{++}\pi^-$ low-mass enhancement can both be described in terms of a Deck-type diagram, a Monte Carlo study indicates that any mechanism that produces particles with limited transverse momentum will yield a $\Delta^{++}\pi^-$ low-mass enhancement.

I. INTRODUCTION

Many investigations have been made in recent years of the inclusive production of single particles and of the mechanisms involved in this production. Fewer studies have been made of the inclusive production of resonances, such as the ρ^0 meson and the $\Delta^{++}(1232)$ baryon. Determining the distributions of resonances in rapidity and transverse momentum, among other variables, and

understanding the similarities to and differences from the distributions of stable particles can lead to an understanding of the fundamental processes involved. The difficulty in studying inclusive resonance production is that there is often a strong background under the resonance which cannot be easily disentangled from the signal. This is especially true in the study of the inclusive ρ^0 distributions at high energies.[1] The Δ^{++} signal has relatively little background, which can be reduced still further by kinematic cuts so that a very clean resonance sample can be obtained and the distributions of this sample studied.

The inclusive production of the Δ^{++} resonance at Fermilab energies has been studied primarily in the reaction

$$pp \to \Delta^{++}(1232)+X, \tag{1}$$

where X stands for "anything".[2] One study reported results with a π^+ beam [Ref. 2(c)] in the reaction

$$\pi^+p \to \Delta^{++}(1232)+X, \tag{2}$$

and preliminary results for

$$\pi^-p \to \Delta^{++}(1232)+X \tag{3}$$

have been given.[3] These reactions have also been studied at medium energies (8–69 GeV/c) in pp,[4] π^+p,[5] and π^-p (Ref. 6) interactions. Those authors who discussed possible production mechanisms found their results consistent with either a one-pion-exchange mechanism[2(b)-2(d)] or with production of the Δ^{++} as the decay product of a higher-mass baryon system.[2(a),6(b)] Some authors have studied the fraction of Δ^{++} which are produced diffractively [Ref. 2(d)].

In this paper we present results on inclusive Δ^{++} production in π^-p interactions at 147 GeV/c. The experimental details are presented in Sec. II. In Sec. III the results are presented in four subsections: III A, the total and differential Δ^{++} cross sections; III B, the energy dependence of Δ^{++} production; III C, evidence for Δ^{++} production via one-pion exchange; III D, evidence for Δ^{++} association with target fragmentation and the kinematic effects of limited transverse momentum particle production. The two pictures of the production mechanism are compared in Sec. IV. The results are summarized and conclusions are given in Sec. V.

II. EXPERIMENTAL DETAILS

This study is based on 105 000 pictures obtained in the Fermilab 30-inch-bubble-chamber–proportional-wire-chamber hybrid spectrometer exposed to a beam of 147-GeV/c mesons. General details of the experimental arrangement and of the data reduction in this experiment have already been published.[7,8] About 16 000 interactions were found within a specified fiducial volume, measured with the automatic precision-encoding and pattern-recognition (PEPR) system and reconstructed with the chain of programs GEOMAT-PWGP-TKORG.[8] Some of the events which were not completely reconstructed from the initial measurement have been remeasured with manually operated machines.

The data sample presented here consists of 6874 successful events originating from either the first measurement or the first half of the remeasured events. A successful event is defined as one which does not violate charge conservation, although a track may be missing because of improper measurement. A total of 3255 tracks out of 46 348 were missing in this sample after linkage with the more precise proportional-wire-chamber information. A weight has been assigned to each histogram entry to correct for the missing tracks in a statistical way; this weight, which is essentially the inverse of a topology-dependent angular efficiency, is equal to the number of tracks actually present in a particular angular interval in the film plane divided by the number of tracks reconstructed in space in the same interval. The Δ^{++} cross sections obtained using these weights are consistent with those obtained without them, i.e., the missing tracks are not associated with the Δ^{++}. This is to be expected since the proton and π^+ forming the Δ^{++} have low momenta in the laboratory and are almost always well measured. The numbers of events in the various topologies have also been corrected for scanning and processing losses by normalization to the topological cross sections presented in Ref. 8.

For this study all negative particles were assumed to be pions. A positive particle having laboratory momentum less than 1.4 GeV/c was identified as a proton or pion by ionization[9]; otherwise, it was assumed to be a pion. An identified proton was required for the Δ^{++} events in this study; the numbers of these events are given in column 2 of Table I as a function of topology. The Δ^{++} cross sections, discussed in detail in Sec. III, are also given in Table I.

In addition to the angular efficiency correction and the corrections discussed in Ref. 8, two further corrections have been made to the Δ^{++} cross sections: (1) for protons with momentum less than 1.4 GeV/c which should have been identified but were not, and (2) for protons with momentum above 1.4 GeV/c. The first of these corrections was determined through an investigation of four-constraint fits to the two-, four-, and six-prong events. A proton identification inefficiency of

TABLE I. Topological distributions of events and the resulting cross sections for $\Delta^{++}(1232)$ production in the reaction $\pi^- p \to \Delta^{++} X$ at 147 GeV/c.

(1) Number of charged prongs	(2) Number of events with identified protons	(3) Number of events with Δ^{++} [a]	$\sigma(\Delta^{++})$ in mb (4) All combinations [b]	(5) Combination with smallest $Y(p\pi^+)$ [b]	(6) Combination with smallest $Y(p\pi^+)$ and $\lvert t_{p\Delta}\rvert<1.0$ (GeV/c)^2 [c]
all	2227	471 ± 60	1.61 ± 0.26	1.56 ± 0.23	1.13 ± 0.16
4	747	137 ± 31	0.38 ± 0.13	0.38 ± 0.13	0.34 ± 0.06
6	620	141 ± 29	0.45 ± 0.09	0.40 ± 0.09	0.26 ± 0.07
8	480	95 ± 30	0.39 ± 0.13	0.41 ± 0.12	0.20 ± 0.08
10	254	67 ± 26	0.40 ± 0.14	0.26 ± 0.10	0.11 ± 0.06
12 – 16	126	6 ± 21	0.08 ± 0.15	0.02 ± 0.12	0.06 ± 0.07

[a] Not corrected for unidentified protons.
[b] Corrected for unidentified protons above and below 1.4 GeV/c as explained in the text.
[c] Corrected for unidentified protons below 1.4 GeV/c as explained in the text.

(1.3 ± 2.6)% has been observed in the four-prong sample, and (4.2 ± 8.2)% in the six-prong sample.[9] The latter figure is believed to apply also to the higher multiplicities. The Δ^{++} cross sections and errors presented in this paper have been increased appropriately. The second correction was determined from the laboratory momentum distribution of identified protons. Figure 1(a) shows the momentum distributions of all the protons in the sample in events having four or more prongs and of all those which have the invariant mass of a $p\pi^+$ combination in the mass range 1.14–1.30 GeV. Figure 1(b) gives the corresponding distributions for the subsample of events with four and six prongs. The momentum distributions in Fig. 1 are quite linear in the momentum range from 0.9 to 1.4 GeV/c, as are the distributions for the higher multiplicities (not shown separately). These regions have been fitted to straight lines, which were then extrapolated to zero events as shown. The areas under the extrapolated lines are assumed to represent the missing protons. From Fig. 1(a) we determined that the number of events in the specified mass range should be increased by (11 ± 6)%. This correction is larger than the corresponding correction (5.8 ± 3)% for the total identified proton sample, indicating that the fraction of high momentum protons from Δ^{++} decay is higher than that for protons from other processes. This correction to Δ^{++} cross sections has been broken down further by considering the 4–6-prong events and the 8–16-prong events separately. The correction factors are (0.8 ± 0.4)% and (20.3 ± 10.2)% for these two groups, respectively. These corrections have been applied to Δ^{++} cross sections where appropriate.

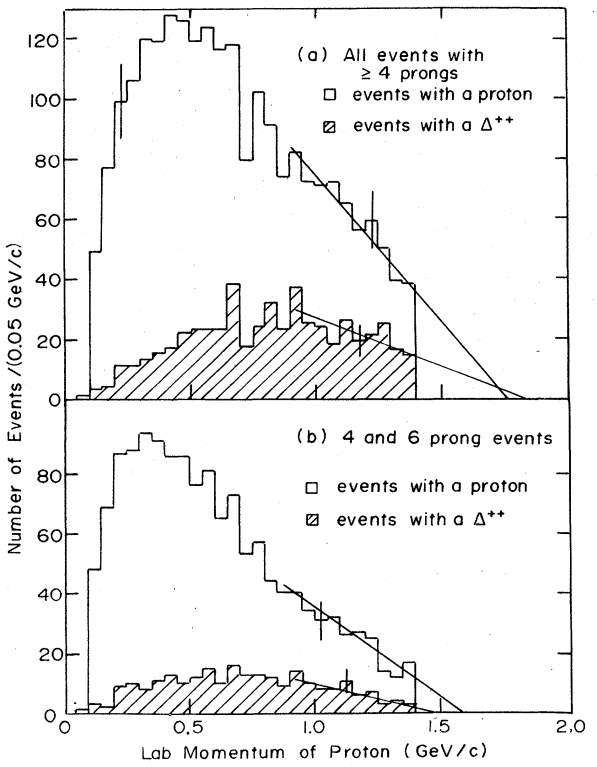

FIG. 1. Laboratory momentum of protons (a) in all events with four or more charged particles (unshaded histogram) and in all events with a Δ^{++} (shaded histogram) and (b) in all events with four or six charged particles (unshaded histogram) and in all events with four or six charged particles and with a Δ^{++} (shaded histogram). The straight lines are the results of the fits discussed in the text.

Another type of correction is needed for any angular analysis of the Δ^{++}. The cut at proton momentum 1.4 GeV/c causes a relative loss in certain regions of the Δ^{++} decay angle unless a further cut of $\lvert t_{p\Delta}\rvert<1.0$ (GeV/c)^2 is applied, where $t_{p\Delta}$ is the square of the four-momentum transfer between the target proton and the Δ^{++}. Consequently, in

the analysis of angular distributions presented in this paper, only events with $|t_{p\Delta}|<1.0$ (GeV/c)^2 have been used. Total Δ^{++} production cross sections are presented both with and without the t cut in Table I.

III. CHARACTERISTICS OF Δ^{++} PRODUCTION

A. Total and differential Δ^{++} cross sections

The unshaded histogram of Fig. 2 is the invariant mass distribution of the $p\pi^+$ system for all events. The only statistically significant structure is a Δ^{++} peak on top of the smooth background. As can be seen in Fig. 2 the amount of background underneath the Δ^{++} resonance is substantial; part of it comes from the combinatorial effects of high-multiplicity events. Several methods to reduce the background by using only one $p\pi^+$ combination per event were tried, and all were found to give similar cross section results. These included selecting the $p\pi^+$ combination having (1) the smallest value of the center of mass rapidity of the combination, (2) the invariant mass of the combination closest to 1232 MeV, (3) the rapidity of the π^+ closest to the rapidity of the proton, (4) the smallest value of the Feynman x of the combination, and (5) the x of the π^+ closest to the x of the proton. The first method has been selected for all subsequent analyses in this study; the justification for this choice is discussed below.

The center-of-mass rapidity distribution of all the $p\pi^+$ combinations, $y^*(p\pi^+)$, is shown in Fig. 3(a). The shaded histrogram in this figure has the additional requirement that the $p\pi^+$ combinations are in the Δ^{++} region, $1.14<M(p\pi^+)<1.30$ GeV. This graph shows that the Δ^{++} tend to be produced at the lowest kinematically-allowed rapidity. Because of this, we have plotted in Fig. 4 the effective mass distributions for the $p\pi^+$ combinations which have the lowest value of $y^*(p\pi^+)$ in each event. The inclusive Δ^{++} mass distribution and the distribution for each topology shown in Figs. 4(a)–4(f), have been fitted to the sum of a Breit-Wigner resonance shape[10] and a third-order polynomial background[11] over an appropriate mass range, usually 1.12–1.92 GeV. The upper curves shown in Fig. 4 are the overall fits and the lower curve in each case is the contribution from the polynomial. The areas between the two curves give the cross sections for Δ^{++} production. The Δ^{++} mass was found to be 1228 ± 6 MeV in a separate fit (not shown) to the full inclusive $p\pi^+$ invariant-mass distribution. The fits made to the displayed distributions yield cross sections for Δ^{++} production consistent with those obtained for the full inclusive distributions. (See columns 4 and 5 in Table I.)

The Feynman-x distribution of the Δ^{++}, which is defined as the $p\pi^+$ combination with the lowest rapidity in the event and with an effective mass in the range 1.14–1.30 GeV, is shown in Fig. 3(b). The shaded histogram has the additional restriction that $|t_{p\Delta}|<1.0$ (GeV/c)^2. As in earlier re-

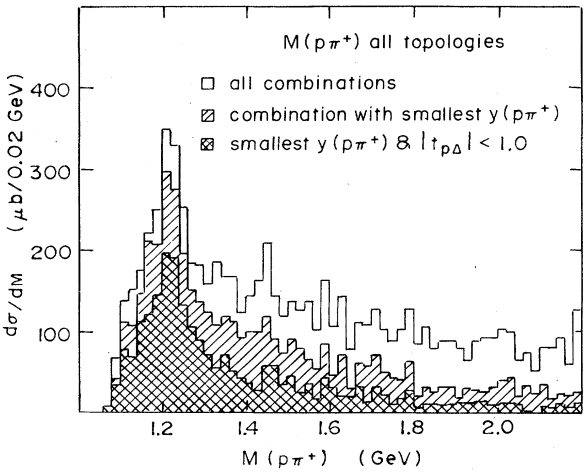

FIG. 2. Effective mass of $p\pi^+$ combinations for all combinations in all events (unshaded histogram), the lowest-rapidity $p\pi^+$ combination in each event (shaded histogram), and the lowest-rapidity $p\pi^+$ combination (cross-hatched histogram) in those events in which that combination had the magnitude of the four-momentum transfer squared from the proton to the $p\pi^+$ combination less than 1 (GeV/c)^2.

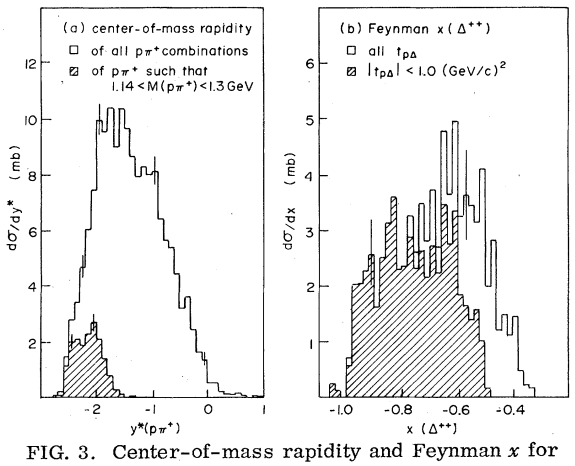

FIG. 3. Center-of-mass rapidity and Feynman x for $p\pi^+$ combinations. The unshaded histogram in (a) is for all $p\pi^+$ combinations and the shaded histogram is for $p\pi^+$ combinations in the Δ^{++} mass region. The histograms in (b) are for the lowest-rapidity $p\pi^+$ combination in events in which that combination has effective mass between 1.14 and 1.30 GeV. The unshaded histogram is for all four-momentum transfers $t_{p\Delta}$ and the shaded one for $|t_{p\Delta}|$ less than 1 (GeV/c)^2.

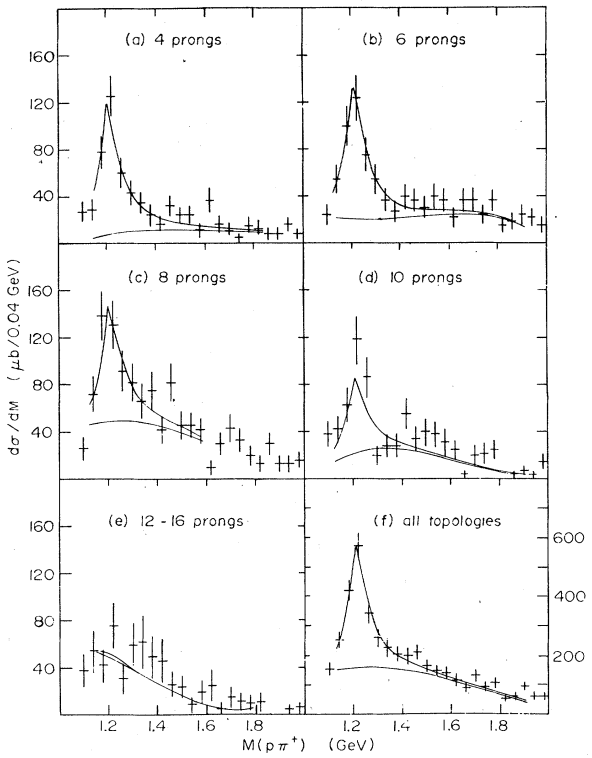

FIG. 4. Effective mass of the lowest-rapidity $p\pi^+$ combination in each event, for each topology. The curves shown are the results of the fits described in the text.

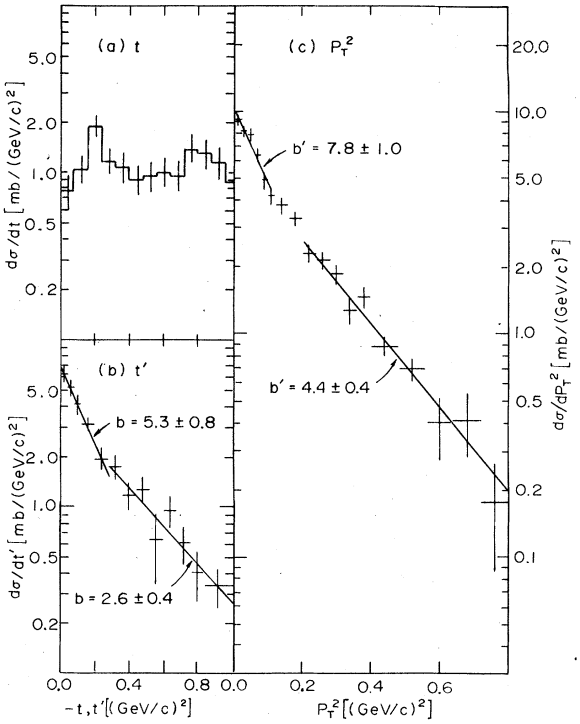

FIG. 5. The square of the four-momentum transfer from the proton to the Δ^{++} is shown in (a), $t' = t - t_{\min}$ in (b), and the square of the momentum transverse to the beam in (c). The Δ^{++} is defined by the mass cut $[1.14 < M(p\pi^+) < 1.30$ GeV] applied to the distribution for the lowest rapidity $p\pi^+$ combination of each event. The lines shown are the fits to $Ae^{bt'}$ and $A'e^{b'P_T^2}$ discussed in the text.

sults for reactions (1) and (3) [Refs. 2(a), 2(b), 2(d), 6(a), 6(b)], no leading Δ^{++} peak is apparent in this distribution.

The $|t_{p\Delta}|$ distribution for the Δ^{++} region is plotted in Fig. 5(a). The unusual flatness of this distribution results from the large $t_{\min}$ values associated with the high masses recoiling against the Δ^{++}. In contrast to this flat t distribution, the distribution in $t' \equiv t - t_{\min}$ shown in Fig. 5(b) has a steep exponential decrease. Fits to the form $d\sigma/dt' = Ae^{bt'}$ yield slopes of $b = 5.3 \pm 0.8$ $(\mathrm{GeV}/c)^{-2}$ over the range $|t'_{p\Delta}| < 0.28$ $(\mathrm{GeV}/c)^2$ and $b = 2.6 \pm 0.4$ $(\mathrm{GeV}/c)^{-2}$ over the range $0.28 < |t'_{p\Delta}| < 0.88$ $(\mathrm{GeV}/c)^2$.

The transverse-momentum P_T^2 distribution for the Δ^{++} region is shown in Fig. 5(c). A fit (not shown) to the expression $d\sigma/dP_T^2 = A'e^{-b'P_T^2}$ over the range $P_T^2 < 0.2$ $(\mathrm{GeV}/c)^2$ yields a slope of $b' = 6.7 \pm 0.5$ $(\mathrm{GeV}/c)^{-2}$. Similar t' and P_T^2 slopes have been found for reactions (1) [Ref. 2(d)] and (3) [Refs. 6(a) and 6(b)] at other energies.

The breaks seen in the 205 GeV/c P_T^2 and t' distributions[2(d)] are apparent in our data as seen in Fig. 5, but our data for both distributions are also consistent with single straight lines. The break in P_T^2 in Fig. 5(c) appears to occur near 0.1 $(\mathrm{GeV}/c)^2$. The slope obtained for $P_T^2 < 0.12$ $(\mathrm{GeV}/c)^2$ is $b' = 7.8 \pm 1.0$ $(\mathrm{GeV}/c)^{-2}$, while for $0.2 < P_T^2 < 0.8$ $(\mathrm{GeV}/c)^2$, the slope is 4.4 ± 0.4 $(\mathrm{GeV}/c)^{-2}$. When the slopes are determined over the wider ranges $|t'| \leq 1.2$ $(\mathrm{GeV}/c)^2$ and $P_T^2 < 0.8$ $(\mathrm{GeV}/c)^2$, we obtain the slopes $b = 3.4 \pm 0.3$ $(\mathrm{GeV}/c)^{-2}$ and $b' = 5.7 \pm 0.3$ $(\mathrm{GeV}/c)^{-2}$.

B. Energy dependence of Δ^{++} production

The cross section for the inclusive production of Δ^{++} in reaction (1) for seven experiments between 12 and 400 GeV/c has been found to vary as $p_{\mathrm{lab}}^{-0.29 \pm 0.03}$ [Ref. 2(d)]. Fewer measurements have been made of the Δ^{++} cross sections for reaction (3). Those measurements which are available have been extracted under such different conditions that a study of the energy dependence of reaction (3) is difficult. A summary of the cross sections obtained at various energies and the conditions of measurement are given in Table II.

The energy dependence for four methods of extraction of the signal is as follows:

(1) The cross section obtained by fitting the

TABLE II. Cross sections (mb) for Δ^{++} production in the reaction $\pi^- p \to \Delta^{++} X$ under various conditions of extraction.

	Incident momentum				
	11.2 GeV/c [Ref. 6(a)]	15 GeV/c [Ref. 6(b)]	16 GeV/c [Ref. 6(c)]	147 GeV/c (this experiment)	205 GeV/c (Ref. 3)
(1) Fit to total distribution		1.3 ±0.1 [a]		1.61±0.26	
(2) $\lvert t\rvert<1.0$ (GeV/c)^2 and $1.12<M(p\pi^+)<1.32$ GeV		1.03±0.11 [b]		1.24±0.07	1.19±0.1
(3) $\lvert t\rvert<0.6$ (GeV/c)^2 and $1.12<M(p\pi^+)<1.36$ GeV			0.71±0.05 [b]	0.85±0.06	0.8 ±0.1
(4) $x(\pi^+)<0$ and $x(p)<0$ and $1.12<M(p\pi^+)<1.32$ GeV	2.1 [b]			2.25±0.09	

[a] Unpublished data, MIT.
[b] Extracted from information given in the referenced paper.

total distribution to an appropriate Breit-Wigner shape over a smooth polynomial background appears constant within errors at 1.3–1.6 mb from 15 to 147 GeV/c.

(2) The cross section for $p\pi^+$ combinations having $\lvert t_{p\Delta}\rvert<1.0$ (GeV/c)^2 and a mass between 1.12 and 1.32 GeV appears constant within errors at 1.0–1.2 mb from 15 to 205 GeV/c.

(3) The cross section for $p\pi^+$ combinations having $\lvert t_{p\Delta}\rvert<0.6$ (GeV/c)^2 and a mass between 1.12 and 1.36 GeV appears constant within errors at 0.7–0.85 mb from 16 to 205 GeV/c.

(4) The cross section for $p\pi^+$ combinations having negative Feynman x for both the proton and the π^+ of the Δ^{++}, and a mass between 1.12 and 1.32 GeV, appears constant within errors at 2.1–2.25 mb from 11.2 to 147 GeV/c.

Thus we conclude that, independent of the method of extraction, the Δ^{++} cross section is consistent with being constant from 15 to 205 GeV/c in reaction (3). The cross sections extracted from the fits (method 1) are more reliable since a mass cut includes a substantial amount of background. Comparing these results with those shown for reaction (1) in Fig. 5 of Ref. 2(d), we observe that (a) both reactions are consistent with energy independence at high energies ($p_{\text{lab}}>50$ GeV/c) and (b) the energy independence of the Δ^{++} cross section extends to lower energies in $\pi^- p$ reactions than in pp reactions.

C. Evidence for Δ^{++} production via one-pion exchange

Most previous studies have found that, in reaction (1), Δ^{++} production is consistent with a one-pion-exchange (OPE) model.[2(b)-2(d)] The evidence which is considered to favor pion exchange as the dominant contribution is (1) the $t'_{p\Delta}$ and $P_T{}^2$ distributions are exponentials with steep slopes, (2) the x distribution of the Δ^{++} has a steep rise near $x=-1$ and a broad maximum near -0.85, consistent with triple-Regge predictions for $\pi\pi$ Pomeron and $\pi\pi$ Reggeon couplings,[12] (3) the spin-density matrix elements obtained for the Δ^{++} decay angular distribution in the Gottfried-Jackson frame are consistent with absorptive OPE in the triple-Regge model,[13] and (4) the properties of the system X in reaction (1) are similar to those of X in $\pi^- p \to X$ reactions at corresponding center-of-mass energies M_X [Refs. 2(b)–2(d)].

The $t'_{p\Delta}$ and $P_T{}^2$ distributions obtained in this experiment, reaction (3), were discussed in Sec. III A and displayed in Fig. 5. We obtained steep slopes consistent with those expected for one-pion exchange.

The x distribution for the Δ^{++} for all $P_T{}^2$ in this experiment [Fig. 3(b)] is consistent with the shape expected for one-pion exchange.

In Figs. 6(a) and 6(b) are displayed the $\cos\theta$ and the ϕ distributions in the Gottfried-Jackson frame for the Δ^{++} region, as defined in Sec. III A, with the cut $\lvert t_{p\Delta}\rvert<1.0$ (GeV/c)^2 to insure unbiased angular distributions. The Δ^{++} decay angular distribution can be expressed in the Gottfried-Jackson frame as

$$w(\theta,\phi)=\left[\frac{3}{4\pi}\,\rho_{33}\sin^2\theta+\rho_{11}(\tfrac{1}{3}+\cos^2\theta)-\frac{2}{\sqrt{3}}\,\mathrm{Re}\rho_{31}\sin 2\theta\cos\phi-\frac{2}{\sqrt{3}}\,\mathrm{Re}\rho_{3(-1)}\sin^2\theta\cos 2\phi\right], \tag{4}$$

where $\rho_{11}=\frac{1}{2}-\rho_{33}$. The density matrix elements can be calculated from the moments of the distribution as follows:

$$\rho_{33}=\tfrac{7}{8}-\tfrac{15}{8}\langle\cos^2\theta\rangle=\tfrac{1}{4}-\left(\frac{5\pi}{4}\right)^{1/2}\langle Y_{20}\rangle, \tag{5}$$

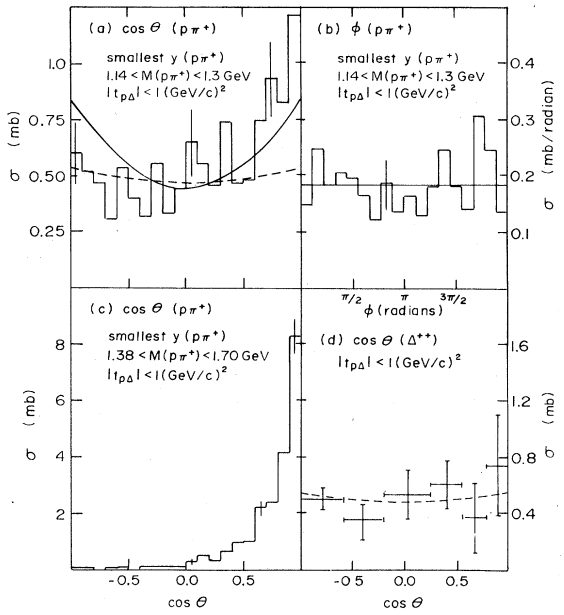

FIG. 6. The (a) $\cos\theta$ and (b) ϕ distributions in the Gottfried-Jackson frame for $p\pi^+$ combinations in the Δ^{++} sample. The $\cos\theta$ distribution for lowest rapidity $p\pi^+$ combinations which have effective masses above the Δ^{++} mass is shown in (c). The $\cos\theta$ distribution for the Δ^{++} alone, as obtained from fits to the $p\pi^+$ mass distribution in the various $\cos\theta$ regions, is shown in (d). The solid curves are $w(\theta)$ and $w(\phi)$ for $\rho_{33}=0.13$ and $\mathrm{Re}\,\rho_{3-1}=0$, and the dashed curves are for $\rho_{33}=0.23$, as discussed in the text.

$$\mathrm{Re}\rho_{31} = -\frac{5\sqrt{3}}{8}\langle \sin 2\theta \cos\phi\rangle = \left(\frac{5\pi}{2}\right)^{1/2}\langle Y_{21}\rangle, \quad (6)$$

$$\mathrm{Re}\rho_{3(-1)} = -\frac{5\sqrt{3}}{8}\langle \sin^2\theta \cos 2\phi\rangle = -\left(\frac{5\pi}{2}\right)^{1/2}\langle Y_{22}\rangle, \quad (7)$$

or they can be determined from fits to the $\cos\theta$ and the ϕ angular distributions,

$$w(\theta) = (\tfrac{1}{4}+\rho_{33}) + 3(\tfrac{1}{4}-\rho_{33})\cos^2\theta, \quad (8)$$

$$w(\phi) = \frac{1}{\pi}\left(\tfrac{1}{2} - \frac{2}{\sqrt{3}}\mathrm{Re}\rho_{3(-1)}\cos 2\phi\right). \quad (9)$$

The results from the method of moments (presented in Table III, Row 1) are consistent with the pp results[2(b)-2(d)] and with the absorptive OPE predictions.[13] The density matrix elements have been determined for low $|t'|$ and as a function of $|t|$, and the results are listed in Table III. The errors are large, but the trend is toward values expected for pure one-pion exchange at low $|t|$ and $|t'|$. The solid curves shown in Figs. 6(a) and 6(b) are the values of $w(\theta)$ and $w(\phi)$ using the measured values of the density matrix elements from the method of moments, $\rho_{33}=0.13$ and $\rho_{3-1}=0$. The curves have been normalized to the cross section for $-1<\cos\theta<1$. The Treiman-Yang (ϕ) distribution is consistent with the isotropy predicted by OPE; however, the $\cos\theta$ distribution of Fig. 6(a) shows a forward peaking rather than the expected symmetric distribution. This asymmetry may be

TABLE III. Density matrix elements for the Δ^{++} decay in the reaction $\pi^- p \to \Delta^{++} X$ at 147 GeV/c, compared to $pp \to \Delta^{++} X$ at 205 GeV/c and to theoretical predictions.

	ρ_{33}	$\mathrm{Re}\rho_{31}$	$\mathrm{Re}\rho_{3(-1)}$
(1) $\pi^- p \to \Delta^{++} X$ (147 GeV/c) from moments [a]			
Δ^{++} mass cut, $\lvert t\rvert<1.0$	0.13 ± 0.03	0.00 ± 0.03	0.00 ± 0.03
$\lvert t'\rvert<0.2$	0.08 ± 0.04	-0.02 ± 0.04	0.00 ± 0.04
$\lvert t\rvert<0.2$	-0.06 ± 0.07	0.05 ± 0.07	-0.07 ± 0.07
$0.2<\lvert t\rvert<0.4$	0.10 ± 0.06	-0.05 ± 0.07	0.08 ± 0.06
$0.4<\lvert t\rvert<0.6$	0.18 ± 0.08	-0.05 ± 0.08	-0.01 ± 0.06
from fits [a]			
Δ^{++} mass cut, $\lvert t\rvert<1.0$			
$-1<\cos\theta<1$	0.15 ± 0.03		
$-1<\cos\theta<0.6$	0.23 ± 0.04		
Δ^{++} cross section, $\lvert t\rvert<1.0$			
$-1<\cos\theta<1$	0.23 ± 0.07		
(2) $pp \to \Delta^{++} X$ (205 GeV/c) [b]	0.11 ± 0.04	0.01 ± 0.04	0.02 ± 0.04
(3) Pure OPE prediction	0	0	0
(4) Absorptive OPE prediction [c]	0.12	0.06	0.03

[a] As explained in the text. [b] Reference 2(d). [c] Reference 13.

due to the background remaining under the resonance signal in the Δ^{++} region, as can be seen in Fig. 6(c) where the same $\cos\theta$ distribution is plotted for a mass region above the Δ^{++} [$1.38 < M(p\pi^+) < 1.70$ GeV]. This distribution is very strongly peaked in the forward direction, with no contribution in the backward hemisphere. To eliminate the effect this background has on ρ_{33}, we have fitted the $\cos\theta$ distribution over the range $-1 < \cos\theta < 0.6$ and display the result ($\rho_{33} = 0.23$) as the dashed curve in Fig. 6(a).

A second way of eliminating the background effect is to obtain the actual Δ^{++} distribution in $\cos\theta$ by fitting the $M(p\pi^+)$ distributions for various $\cos\theta$ slices to a Δ^{++} resonance plus background parametrization, as discussed in Sec. III A. In Fig. 6(d), we present the Δ^{++}-resonance cross sections resulting from these fits; this is the actual Δ^{++} distribution, with no background contamination. This distribution is more symmetric than the one obtained with a simple mass cut. The value of ρ_{33} obtained from fitting this distribution (0.23) is identical to that obtained from fitting the mass cut data for $\cos\theta < 0.6$. The values of ρ_{33} obtained from these data are not very accurate but are consistent with one-pion exchange.

If the Δ^{++} production can be viewed as occurring via the exchange of some object E^- (such as a π^-) as shown in the inset in Fig. 7 for reaction (3), one can study the off-mass-shell inclusive processes

$$E^- + p \to \pi^- + X', \tag{10}$$

$$E^- + \pi^- \to \pi^- + X', \tag{11}$$

in reactions (1) and (3), respectively, as a function of center-of-mass energy M_X. In reactions (10) and (11), E^- is the exchanged object and X' is the system recoiling against the Δ^{++} and the π^-, i.e., the X of reactions (1) and (3) are the $\pi^- + X'$ of reactions (10) and (11), respectively. The inclusive invariant x distribution of the π^- in reaction (10) was found[2(b)] to be consistent with the inclusive π^- distributions from $\pi^- p$ interactions at s values similar to the M_X^2 values of reaction (10). Thus, the authors of Ref. 2(b) conclude that the internal properties of the system X of reaction (1) [i.e., the $\pi^- + X'$ of reaction (10)] are similar to those expected from the emission of a virtual π^- meson [the E^- of reaction (10)] which subsequently interacts with the second incident proton. That is, the observation that $E^- p$ interactions are identical to $\pi^- p$ interactions leads to the conclusion that the E^- may be regarded as a π^-.

We have examined our Δ^{++} sample, which has a 27% background under the Δ^{++} signal, for properties of $E^-\pi^-$ scattering. Figure 8 shows the cross section for Δ^{++} production as a function of M_X^2. The distribution appears to be flat for M_X^2 above

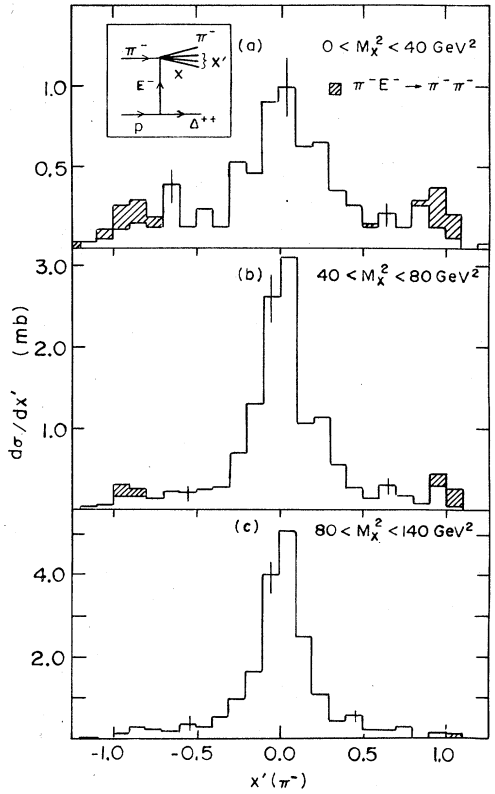

FIG. 7. The inclusive x' distribution for π^- produced in $\pi^- E^-$ interactions, as described in the text. The shaded events are the contributions from $\pi^- p \to p\pi^+\pi^-\pi^-$ events.

10 GeV^2 up to the kinematic cutoff. If factorization is valid, this indicates that the $E^-\pi^-$ total cross section is independent of the center-of-mass energy M_X at high energies.

We have also examined the inclusive x distribution of the π^- in reaction (11). If the picture is valid, and if E^- is indeed a π^-, we should be able

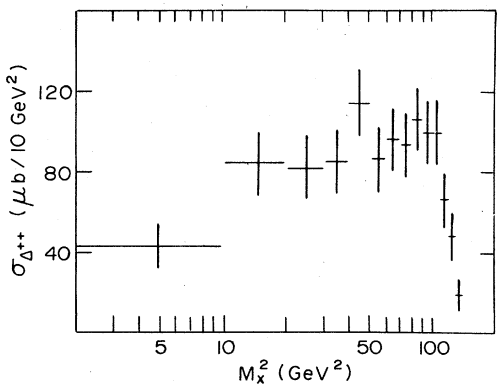

FIG. 8. Cross section for Δ^{++} production as a function of mass M_X^2 recoiling off the Δ^{++}.

to extract some information on leading-particle effects in $\pi^-\pi^-$ scattering. Figures 7(a)–7(c) contain the x distributions of the outgoing π^- of reaction (11) in the $E^-\pi^-$ center of mass, or the rest frame of the X of reaction (3), for events having a $p\pi^+$ in the Δ^{++} sample with $|t_{p\Delta}|<1$ (GeV/c)^2. The t cut serves the purpose of removing angular biases, as before, and also tends to enhance any π-exchange present. The three distributions are for three regions of center-of-mass energy M_X as indicated in the figures. The incident E^- direction is as defined in Ref. 2(b) so that negative x' corresponds to emission along the direction of the beam π^-. The x' variable is defined as

$$x'(\pi^-)\equiv 2M_X P_L/\{[M_X^2-(N+1)^2 m_\pi^2]\times[M_X^2-(N-1)^2 m_\pi^2]\}^{1/2}$$
$$=2P_L/(M_X^2-4m_\pi^2)^{1/2}, \qquad (12)$$

where P_L is the longitudinal momentum of the π^-, measured along the negative of the incident π^- beam direction in the $E^-+\pi^-$ rest frame, m_π is the pion mass, and $N=1$ is the minimum number of π's which can recoil against the π^- of interest in the π^-+X' system. M_X is the mass recoiling against the Δ^{++}. The symbol x' is used in the subsequent discussion to distinguish this Feynman variable [measured in the center-of-mass of reaction (11)] from the x evaluated in the center-of-mass of reaction (3).

A leading-particle effect is apparent in Fig. 7 near $x'=1$ for the lower values of M_X, which have low $\langle n_X\rangle$, but is not apparent at the highest M_X values which have high $\langle n_X\rangle$. The relationship between M_X and $\langle n_X\rangle$ is discussed in Refs. 2(b), 2(c), 3. The resolution in x' is worse near $x'=-1$, since that corresponds to pions which have very high momentum in the laboratory. This problem is discussed in more detail in Ref. 7. The leading particle effect is also present in this kinematic region.

Part of the leading-particle effect in Fig. 7 corresponds to elastic $\pi^-\pi^-$ scattering, that is, to events from the reaction

$$\pi^- p \to \Delta^{++}\pi^-\pi^-. \qquad (13)$$

The events which had a four-constraint fit to the reaction

$$\pi^- p \to p\pi^+\pi^-\pi^- \qquad (14)$$

and also satisfied the Δ^{++} cuts used are shown as the shaded portions of Figs. 7(a)–7(c). Details of the kinematic-fitting procedure can be found in Ref. 14. When these events are removed, the leading effects are smaller but still present.

The invariant x' distribution, divided by the total cross section for the appropriate M_X^2 range, is shown in Fig. 9. The events below $x'=-1$ and above $x'=+1$ have been included in the first and last bins, respectively, of the invariant distribution. The leading peak in the E^- direction is very strong as is seen in reaction (10) in Ref. 2(b). In contrast to reaction (10), however, a leading peak due to the π^- beam is apparent at $x'=-1$ for reaction (11) in this experiment. The leading peak weakens relative to the central peak at high M_X^2; high M_X^2 corresponds to high $|t_{p\Delta}|$ as can be seen in Fig. 10. Thus, the leading effect in $E^-\pi^-$ scattering, which is most apparent at low M_X^2, appears to be confined to the low $|t|$ values where one expects pion exchange to dominate. The leading peak at $x'=+1$ will be discussed further in Sec. IV.

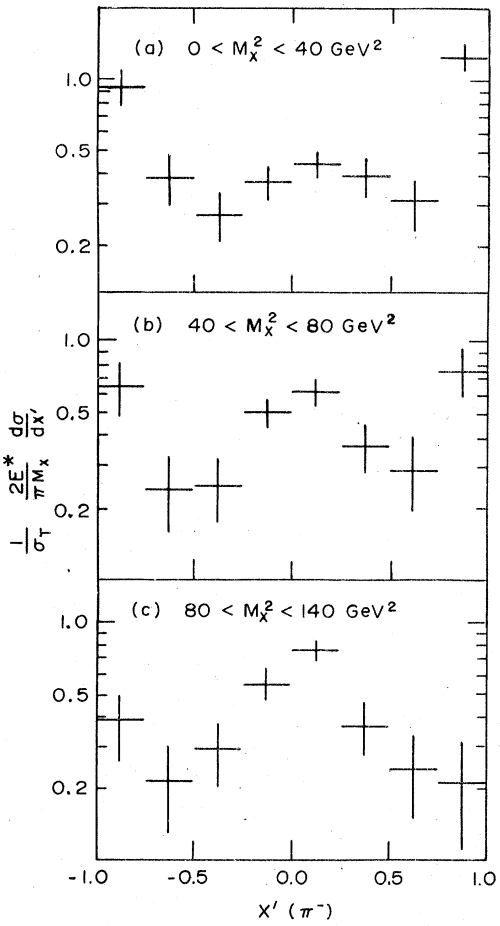

FIG. 9. The invariant x' (π^-) distribution for $\pi^- E^-$ interactions, as described in the text.

To summarize briefly the Δ^{++} phenomena studied in this section, we find that the data are consistent with one-pion-exchange-model predictions with respect to t, P_T^2, x, and decay angular distributions. In addition, the fact that the $x'(\pi^-)$ distribution is symmetric for the off-mass-shell process (11) in-

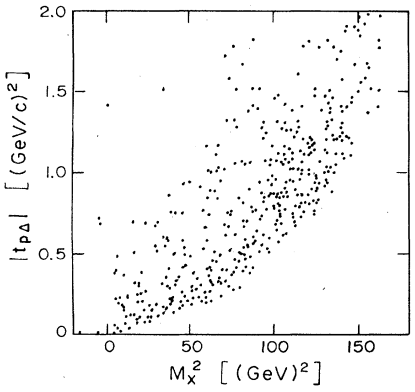

FIG. 10. Correlation between $|t_{p\Delta}|$ and mass M_X recoiling against the Δ^{++} in reaction (3).

dicates that the interpretation of the exchanged object E^- as a π^- is plausible.

D. Evidence for Δ^{++} association with target fragmentation

In Sec. III C we presented evidence that one-pion exchange might dominate in Δ^{++} production. There is also evidence that some Δ^{++} are produced as the decay product of a higher-mass system.[2(a),6(b)] For example, the effective mass of the $\Delta^{++}\pi^-$ system, shown as the unshaded histogram in Fig. 11(a), has a low-mass enhancement typical of diffractive phenomena.[15] We would like to know the extent to which the Δ^{++} is associated with a low-mass $\Delta^{++}\pi^-$ system and the properties of this system. The fact that choosing the lowest-rapidity $p\pi^+$ combination in each event reduced the background under the Δ^{++} without significantly diminishing the Δ^{++} signal leads us to try a similar scheme for the $\Delta^{++}\pi^-$ combinations. The shaded histogram in Fig. 11(a) is the effective mass of all $p\pi^+\pi^-$ combinations such that the $p\pi^+$ mass is in the Δ^{++} region, the $p\pi^+$ rapidity is the lowest in the event, and the π^- is the lowest rapidity negative meson in the event. The low-mass enhancement is more prominent, with relatively few events above 3 GeV. This latter histogram is displayed by topology in Figs. 11(b)–11(e). The shapes of the distributions are the same for all topologies, suggesting that a large fraction of the Δ^{++} in all topologies might be the decay product of a higher-mass system.

We can examine the fraction of Δ^{++} produced in conjunction with a low-mass $\Delta^{++}\pi^-$ system in a complementary way by examining how many low-mass $p\pi^+\pi^-$ systems are or are not associated with a Δ^{++} rather than by asking, as in Fig. 11, how many Δ^{++} are associated with a $\Delta^{++}\pi^-$ system. Figure 12 is the result of asking this question; it shows the effective mass of the lowest-

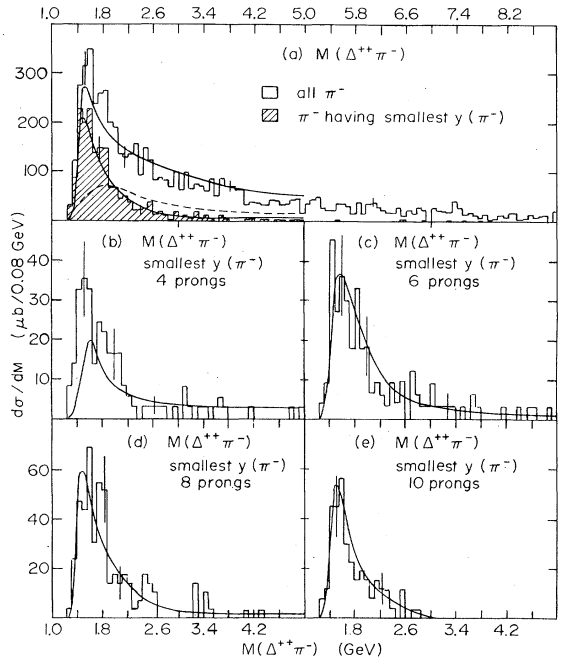

FIG. 11. Effective mass of $\Delta^{++}\pi^-$. The distribution for all π^- is the unshaded histogram in (a). All other histograms shown are for the lowest rapidity π^- in each event with a Δ^{++}. The solid curves shown are for Monte Carlo events with a limited P_T^2 distribution on the non-Δ^{++} pions as described in the text. The dashed curve is for Monte Carlo events with the non-Δ^{++} pions produced uniformly in Lorentz-invariant phase space.

rapidity $p\pi^+$ combination for each event in which any π^- formed a low-mass (less than 2.68 GeV) $p\pi^+\pi^-$ system with this $p\pi^+$. Since it is difficult to tell the fraction of Δ^{++} remaining in this histogram, we show the remainder of the total lowest-rapidity $p\pi^+$ mass distribution in the shaded histogram; i.e., the shaded histogram of Fig. 12 is the effective mass of the lowest rapidity $p\pi^+$ combination for each event in which no π^- formed a low-mass $p\pi^+\pi^-$ system with the $p\pi^+$. Over 90% of the Δ^{++} are associated with a low-mass $\Delta^{++}\pi^-$ system with mass less than 2.68 GeV. It is interesting to note that a similar plot (not shown) made for a $p\pi^+\pi^-$ mass cut of 4 GeV indicates that essentially 100% are associated with a $\Delta^{++}\pi^-$ system with mass less than 4 GeV.

The different shapes of the high-mass tails in the shaded vs unshaded distributions of Fig. 12 are kinematic and phase-space consequences of the $p\pi^+\pi^-$ cuts defined: The unshaded distribution has a kinematic cutoff at a $p\pi^+$ mass of 2.68 GeV, beyond the edge of the graph; the shaded distribution has no such kinematic cutoff. Thus, the nonresonant $p\pi^+$ background in the shaded histogram may grow with $p\pi^+$ mass whereas the nonresonant

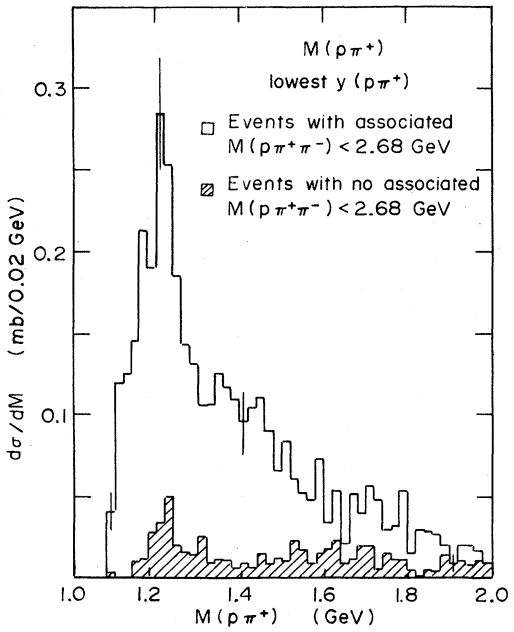

FIG. 12. Effective mass of lowest-rapidity $p\pi^+$ combinations in events in which at least one π^- combined with the $p\pi^+$ to give a $p\pi^+\pi^-$ mass less than 2.68 GeV (unshaded histogram) and for events in which all π^- gave a $p\pi^+\pi^-$ mass greater than 2.68 GeV (shaded histogram).

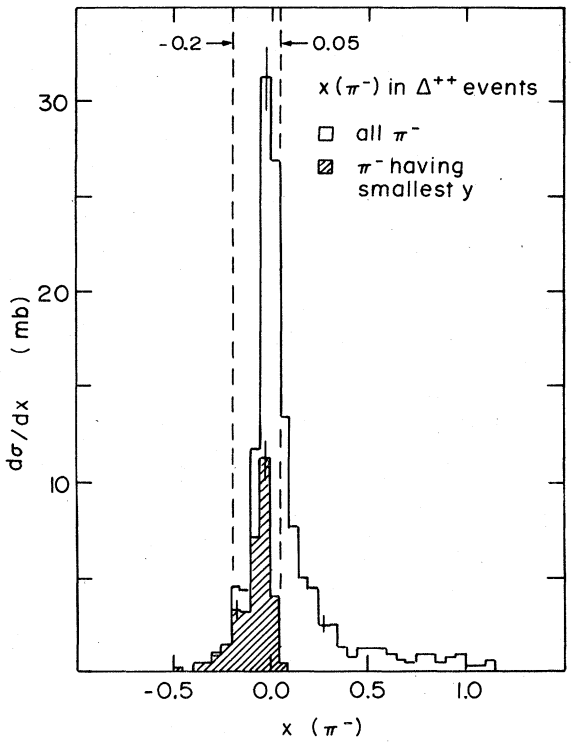

FIG. 13. Feynman x for all π^- in events with a Δ^{++} (unshaded histrogram) and for the lowest-rapidity π^- in each event with a Δ^{++} (shaded histogram). The dashed lines indicate the cut used in Ref. 6(b) to enhance the $\Delta^{++}\pi^-$ signal.

$p\pi^+$ background in the unshaded histogram is required to fall to zero.

The different shapes of the nonresonant low-mass portions of the distributions in Fig. 12 indicate that for a given low $p\pi^+$ mass, it is more likely that there is a nearby π^- forming a low-mass $p\pi^+\pi^-$ combination than that there is none. This is a consequence of the mechanism leading to the $\Delta^{++}\pi^-$ low-mass enhancement, which will be discussed in more detail later.

The observation of a $\Delta^{++}\pi^-$ low-mass enhancement associated with the lowest rapidity π^- in this experiment is consistent with the conclusion of Ref. 6(b), where a cut of $-0.2 < x(\pi^-) < 0.05$ was used to study the $\Delta^{++}\pi^-$ low-mass enhancement. The $x(\pi^-)$ distribution for all π^- in events with a Δ^{++} is shown in Fig. 13 (unshaded histogram), along with the distribution for only the lowest rapidity π^- in events with a Δ^{++} (shaded histogram). Almost all of the latter distribution is concentrated in the region $-0.2 < x(\pi^-) < 0.05$ (dashed lines), indicating that the x cut used in Ref. 6(b) is kinematically equivalent to the lowest rapidity π^- cut used in this experiment.

In an effort to determine whether kinematic effects at this energy could produce a $\Delta^{++}\pi^-$ low-mass enhancement, we ran several Monte Carlo simulations of Δ^{++} production using SAGE[16] and applied the same analysis techniques and cuts to the Monte Carlo events as we had applied to the real events. The number of events thrown in each topology was proportional to the cross section for Δ^{++} production in that topology. The multiplicity distribution of neutral pions for each charged topology was assumed to have the same shape as the multiplicity distribution of all charged pions (Fig. 15), with the average number of produced neutral pions assumed to be equal to the average number of produced positive pions. That is, the average number of π^0's associated with four charged particles for example (a Δ^{++} and two π^-'s) was assumed to be 1.

Monte Carlo events distributed uniformly in phase space did not reproduce any of the Δ^{++} distributions discussed in this paper. Thus, the $\Delta^{++}\pi^-$ low-mass enhancement (Fig. 11) and the x' distributions (Fig. 7) are not simply the consequence of momentum and energy conservation; some dynamics must be included to reproduce them.

Another Monte Carlo simulation we made had a t' slope of 3.4 $(\mathrm{GeV}/c)^{-2}$ on the Δ^{++} and included a cut on $|t_\Delta| < 1$ $(\mathrm{GeV}/c)^2$. Again, the simulation did not match the data; the dashed curve in Fig. 11(a) is the Monte Carlo result for the shaded

histogram, normalized to the same total area.

The third simulation we tried had the same properties for the Δ^{++} produced as the second simulation and in addition assumed that all pions produced in the event were randomly distributed according to $\exp[-(N-1)P_T^2/Na^2]$, where $a=0.562$ GeV/c, N is the number of pions produced in the event, and P_T^2 is the transverse momentum squared in the rest frame of the system recoiling off the Δ^{++}. The distributions obtained with these restrictions qualitatively reproduced the data, including the $\Delta^{++}\pi^-$ low-mass enhancement in all topologies and the nearly symmetric structure in the x' distributions. The smooth curves shown in Fig. 11 are the results of this third Monte Carlo simulation. It is of interest to note that the Monte Carlo distributions for $x'(\pi^+)$ were narrower than the $x'(\pi^-)$ distributions for both of the latter two simulations, indicating that the difference between the π^+ and π^- distributions observed in Ref. 17 might be a phase-space consequence of removing the two lowest rapidity positive particles while including all negative particles.

Several variations on these three basic Monte Carlo simulations were tried with similar results, leading us to conclude that any dynamical model which results in small transverse momenta of the produced particles, such as the multiperipheral diagram discussed in the next section, will have a $\Delta^{++}\pi^-$ low-mass enhancement as a kinematic consequence.

In order to further discuss the $\Delta^{++}\pi^-$ low-mass enhancement, we must clarify which processes are being considered. We will be discussing the reaction:

$$\pi^- p \to p^* X, \tag{15}$$

where p^* is a low-mass, charge +1, isospin $\frac{1}{2}$ baryon system produced at low rapidity. The phrase "target fragmentation" will be used to refer to such a process without regard to the mode of decay of the p^* or to the properties of the system (X) recoiling against it. "Diffraction" will be used to indicate that the system X consists of a single π^- which has Feynman x near 1.

The fact that essentially all of the Δ^{++} are associated with a $\Delta^{++}\pi^-$ low-mass enhancement does not mean that they are all made via reaction (15) with subsequent decay of the p^* directly into $\Delta^{++}\pi^-$; if this were indeed the case, the x distribution for the $\Delta^{++}\pi^-$ system would be sharply peaked near -1. As can be seen in Fig. 14, this is not the case for the $\Delta^{++}\pi^-$ combinations selected by using the π^- with lowest rapidity. Although the $\Delta^{++}\pi^-$ [unshaded histogram of Fig. 14(b)] are clustered at lower x than the full inclusive $x(p\pi^+\pi^-)$ distribution [Fig. 14(a)], there is no strong leading

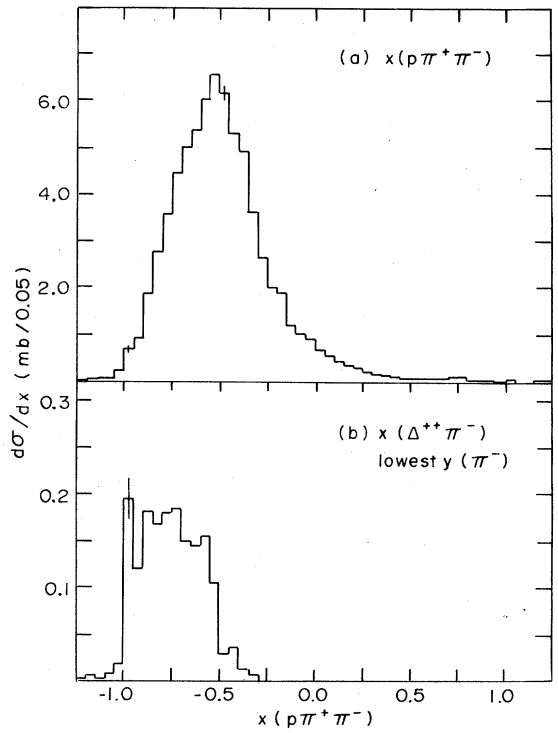

FIG. 14. Feynman x of (a) all $p\pi^+\pi^-$ combinations and (b) $\Delta^{++}\pi^-$ combinations with lowest-rapidity π^-.

peak. It may be that the Δ^{++} are made via reaction (15), but, if so, the p^* then decays to a Δ^{++} and more than one pion part of the time. As many people have shown (e.g., Ref. 7) and the authors of Ref. 2(d) point out, diffraction as defined above occurs only at low multiplicities, six-prong and lower topologies, whereas Δ^{++} production (and, as we see in Fig. 11, the $\Delta^{++}\pi^-$ low-mass enhancement) is apparent in higher topologies as well. Several more recent papers[18] have presented evidence that low and high multiplicity particle production occurs via clusters of low multiplicity and suggest that diffractive (or leading particle) effects occur when only two clusters are present, one of which consists of only one particle.[18(d)] If the $\Delta^{++}\pi^-$ system were produced as part of such a cluster in the target region, with other clusters being produced in the central and beam regions in the event as well, then the Δ^{++} cross section could extend to high multiplicities, whereas the subset of Δ^{++} produced diffractively (i.e., in association with a π^- near $x=1$) would be confined to low multiplicities.

One of these recent papers[18(c)] studied the $p\pi^-$ low-mass enhancement from a neutron target, analogous to the $\Delta^{++}\pi^-$ low-mass enhancement from a proton target which is being discussed here. The $p\pi^-$ low-mass enhancement was found to be produced in all multiplicities with an average mul-

tiplicity $\langle n \rangle$ similar to the total $\langle n \rangle$ of that experiment. In Fig. 15 we show the inelastic cross sections,[8] the Δ^{++} cross sections, and the leading particle cross sections for this experiment[7,19] as functions of topology. The average multiplicity $\langle n \rangle$ of Δ^{++} production (and thus of the $\Delta^{++}\pi^-$ low-mass enhancement) is the same as the total inelastic $\langle n \rangle$ in this experiment, in agreement with the $p\pi^-$ low-mass enhancement of Ref. 18(c). In contrast, the leading particle $\langle n \rangle$, or $\langle n \rangle$ for diffractively produced particles, is about half the total $\langle n \rangle$. The $\langle n \rangle$ for Δ^{++} production as a function of $M_X{}^2$ in this experiment will be discussed in more detail in a forthcoming paper.

IV. COMPARISON AND DISCUSSION

We have seen in Sec. III C that inclusive Δ^{++} production is consistent with an absorptive one-pion exchange model,[13] even at this high energy. In Sec. III D, we saw that essentially all of the Δ^{++} in all topologies were associated with a low-mass $\Delta^{++}\pi^-$ enhancement. As noted in that section, any mechanism that limits the transverse momentum of produced particles will yield such a $\Delta^{++}\pi^-$ low-mass enhancement. One way of producing such a low-mass enhancement is Δ^{++} production via target fragmentation into $\Delta^{++}\pi^-$ (plus any number of charged or neutral pions). This mechanism and a one-pion-exchange mechanism are both compatible with a diagram of the sort shown in Fig. 16. In this diagram, the production of the $\Delta^{++}\pi^-$ system is represented by the exchange of an effective Regge trajectory α, and the interaction between the Δ^{++} and the π^- is represented by an amplitude M. The amplitude M for the $\Delta^{++}\pi^-$ low-mass enhancement should contain a term for pion exchange and a term for N^* production, perhaps similar to the amplitudes found in diffractively produced nucleon-pion low-mass enhancements (i.e., when α is the Pomeron trajectory and X' is a single π^-) at other energies.[20] Some authors have replaced the amplitude M by an effective trajectory of α',[5] using a triple-Regge formalism, and conclude that at least two trajectories having different t-dependences are needed, or at least two terms are needed in the amplitude M. It is well known from studies of a Deck model[21] or a double peripheral model[23] than when a π is exchanged at the lower vertex of the diagram (i.e., when α' is the pion trajectory), a kinematic low-mass enhancement results between the two particles at the bottom of the diagram, which are Δ^{++} and π^- in this case.

It is interesting to note that a theoretical attempt has been made to describe properties of inclusive Δ^{++} production by assuming that the Δ^{++} is a decay product of a diffractively produced system.[23] Using a sum of diffractively produced N^*'s and the Mueller-Regge formalism, the authors of Ref. 23 were able to reproduce the $\Delta^{++}\pi^-$ low-mass enhancement, the x and the steep $P_T{}^2$ distributions of the Δ^{++}, and the peak near $x'(\pi^-) = 1$ of reaction (10), which in Sec. III C was attributed to properties of virtual $\pi^- p$ scattering. One can speculate that if the Δ^{++} are produced via reaction (15) but the final decay product involves more than one pion, the Feynman x of the $\Delta^{++}\pi^-$ low-mass enhancement portion of the p^* would extend to higher x, as in Fig. 14(b), and the effect would extend to higher multiplicities, as in Fig. 11. The Pomeron would still be involved in the production as part of the X' of Fig. 16 and therefore account for

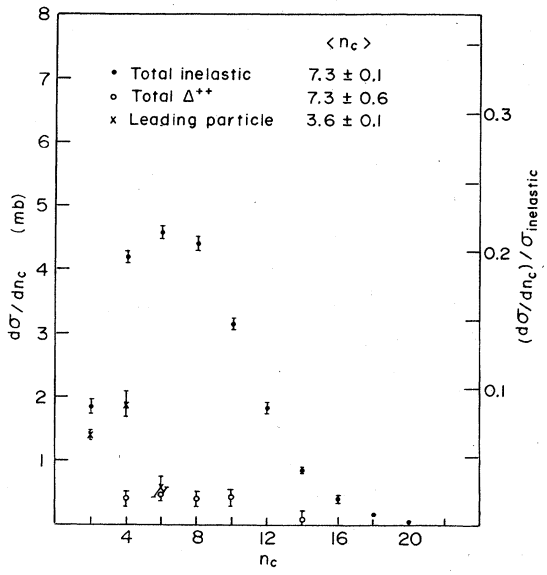

FIG. 15. Inelastic, Δ^{++}, and leading-particle cross sections as functions of topology for $\pi^- p$ interactions at 147 GeV/c.

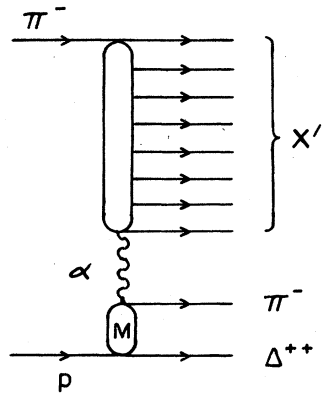

FIG. 16. Diagram for Δ^{++} production which includes both one-pion-exchange and N^*-production amplitudes, as discussed in the text.

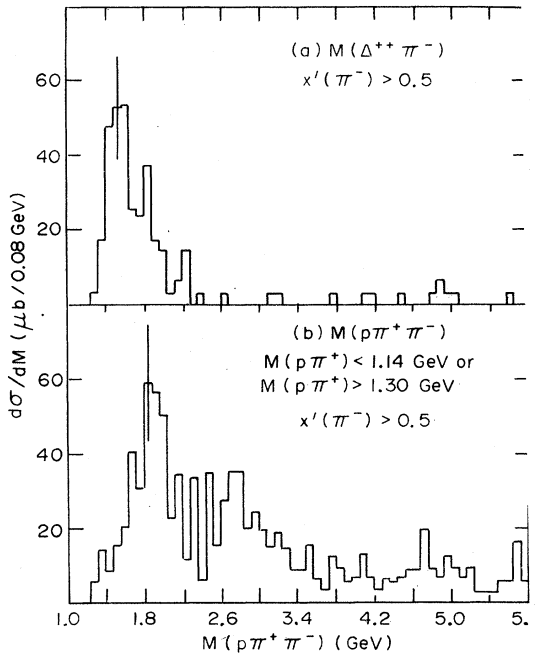

FIG. 17. Effective mass of $p\pi^+\pi^-$ for events in which $x'(\pi^-)$ is greater than 0.5. The $\Delta^{++}\pi^-$ combinations are shown in (a) and the $p\pi^+\pi^-$ combinations outside the Δ^{++} mass region are shown in (b). In both figures, the lowest-rapidity $p\pi^+$ combination was used.

the constancy of the Δ^{++} cross section as a function of energy.

As a further test of the nature of the $x'(\pi^-)=+1$ peak apparent in Figs. 7 and 9, we have plotted in Fig. 17(a) the invariant mass of the Δ^{++} combined will all π^- which have $x'>0.5$. A low-mass enhancement is present, but the shape is the same as that of the total $\Delta^{++}\pi^-$ low-mass enhancement [Fig. 11(a)]. In addition, the x distribution for these π^-, which have $x'>0.5$, is similar to the x distribution for the lowest rapidity π^- shown as the shaded histogram in Fig. 13. It should be noted that only ~25% of the Δ^{++} have $x'(\pi^-)>0.5$. With the small number of events in this experiment, we can draw no conclusions about the relative ratios in this sample of $N^* \to \Delta^{++}\pi^-$ production and of $\Delta^{++}\pi^-$ low-mass enhancement due to a Deck effect.[21] There are contributions to the $x'>0.5$ region from 4–12 prongs, with the four prongs contributing the greatest portion of the peak structure at $x'=1$ but only about half of the total $x'>0.5$ region. The four-prong events which had a four-constraint fit to reaction (14) contribute only about a third of the peak and about a sixth of the total $x'>0.5$ region. Hence, the high topologies furnish the bulk of the events in this region.

The peaks in x' at ±1 are also apparent for $p\pi^+$ masses outside of the narrow mass range defining our Δ^{++} sample. To investigate this we plotted the effective mass of all $p\pi^+\pi^-$ combinations which satisfied the following criteria: (a) the $p\pi^+$ combination had the lowest rapidity in the event, (b) $|t_{p\pi^+}|<1.0$ (GeV/c)^2, (c) x' of the π^- was greater than 0.5, (d) the effective mass of the $p\pi^+$ was either less than 1.14 GeV or greater than 1.30 GeV. The result, shown in Fig. 17(b), is a $p\pi^+\pi^-$ low-mass enhancement, possibly peaking at higher mass values than the $\Delta^{++}\pi^-$ low-mass enhancement. If this x' cut did indeed isolate N^* production, then one could understand the non-Δ^{++} part of the leading $x'(\pi^-)$ peak since a substantial fraction of the higher mass N^*'s decay directly to $p\pi^+\pi^-$. However, the number of events in this $p\pi^+\pi^-$ low-mass enhancement is consistent with the number which should be present from the tails of the Δ^{++} peak.

These distributions were included in our Monte Carlo study of kinematic and phase-space effects. We found that the $x'(\pi^-)$ distributions could not be reproduced by Lorentz invariant phase-space distributions for the produced pions. However, we did find that a mechanism which produces particles with a limited transverse momentum could produce effects similar to those seen in the data.

In brief, the structure in $x'(\pi^-)$ and the $\Delta^{++}\pi^-$ low-mass enhancement could be produced by the mechanisms proposed; that is, by a mixture of N^* production and one-pion exchange at the lower vertex of Fig. 16. Both of these mechanisms lead to limited transverse momentum for at least some of the produced pions. The effects could also be produced by any mechanism which leads to limited transverse momentum for the produced pions and in addition reproduces the x' distributions. It should be emphasized that no simple Monte Carlo simulation can reproduce all of the features of the Δ^{++} production presented in this paper, but any Monte Carlo model which limits P_T^2 can produce effects similar to those seen in the data.

V. SUMMARY

The properties of inclusive Δ^{++} production studied in this paper can be interpreted as either from one-pion exchange at the lower vertex of the diagram shown in Fig. 16 or as resonance formation at the lower vertex. Monte Carlo simulations of the data indicate that an alternate explanation might be supplied by a dynamic model which results in limited transverse momentum of the final-state particles. The Δ^{++} properties found are summarized below.

Inclusive production of the Δ^{++} (1232) resonance in π^-p interactions at 147 GeV/c occurs in comparable amounts in four-, six-, eight-, and ten-prong events, indicating that Δ^{++} production is not as-

sociated entirely with single diffraction of the proton target. The Δ^{++} production cross section in $\pi^- p$ collisions is approximately independent of energy between 11 and 205 GeV/c, indicating that the Pomeron might dominate in the production, even though Δ^{++} production is not confined to low multiplicities. All of the Δ^{++} are produced backwards in the center of mass, with rapidity and x values close to the lowest possible kinematic limit, and essentially all of the Δ^{++} are associated with a $\Delta^{++}\pi^-$ low-mass enhancement. The t' and P_T^2 distributions of the Δ^{++} events are steep, but not quite as steep as in pp interactions at 205 GeV/c. The Gottfried-Jackson angular distributions of the Δ^{++} are consistent within errors with the one-pion-exchange picture, as found in previous experiments. Inclusive $x'(\pi^-)$ distributions from reaction (11) show peaks near ±1 which can be interpreted as leading peaks from $\pi^-\pi^-$ interactions, or as kinematic effects of a multiperipheral interaction, or as kinematic effects of N^* production processes. The x' peak near +1 appears to be associated with $N^* \to \Delta^{++}\pi^-$ and with $N^* \to p\pi^+\pi^-$. The presence of such N^* resonances can explain steep P_T^2 distributions, as indicated in Ref. 23. Hence, it is conceivable that all of these properties could be explained by a total amplitude M for the $\Delta^{++}\pi^-$ low-mass enhancement which includes amplitudes for both pion exchange at the lower vertex and N^* resonances.

ACKNOWLEDGMENTS

This work was supported in part by the U. S. Department of Energy and the National Science Foundation. We wish to thank the personnel of the Fermilab neutrino section and the 30-inch bubble-chamber facility whose skills and efforts made this experiment possible. We also thank the personnel of the participating universities and our data reduction personnel whose dedicated skills were vital to the success of this work. The authors would like to thank C. E. DeTar for enlightening comments and discussions.

---

*Present address: DESY, Hamburg, West Germany.
†Present address: New England Nuclear, Billerica, Massachusetts.
‡Present address: Polytechnic Institute of New York, Brooklyn, New York.
§Present address: Indiana University, Bloomington, Indiana.
||Present address: Purdue University, West Lafayette, Indiana.
¶Present address: Argonne National Laboratory, Argonne, Illinois.
**Present address: Dialog Systems, Inc., Belmont, Massachusetts.
††Present address: Duke University, Durham, North Carolina.
‡‡On leave of absence from Tel-Aviv University, Israel.
§§Present address: Stanford Linear Accelerator Center, Stanford, California.
||||Present address: Tel-Aviv University, Israel.
¶¶Present address: Weizmann Institute of Science, Rehovot, Israel.
***Present address: Fermilab, Batavia, Illinois.

[1]See, for example, D. Fong *et al.*, Phys. Lett. 60B, 124 (1975).
[2](a) F. T. Dao *et al.*, Phys. Rev. Lett. 30, 34 (1973). (303 GeV/c); (b) J. P. DeBrion *et al.*, *ibid.* 34, 910 (1975). (102, 400 GeV/c); (c) J. Erwin *et al.*, *ibid.* 35, 980 (1975) (100 GeV/c); (d) S. J. Barish *et al.*, Phys. Rev. D 12, 1260 (1975) (205 GeV/c).
[3](a) H. H. Bingham *et al.*, Report No. LBL-3855, 1975 (unpublished) (205 GeV/c); (b) D. Brick *et al.*, report submitted to the XVIII International Conference on High Energy Physics, Tbilisi, U. S. S. R., 1976 (unpublished).
[4](a) Bonn-Hamburg-Munich experiment [quoted by Ref. 2(d)] (12, 24 GeV/c); (b) H. Bialkowska *et al.*, France-Soviet Union Collaboration [quoted by Ref. 2(d)] (69 GeV/c).
[5]J. V. Beaupré *et al.*, Nucl. Phys. B67, 413 (1973) (8, 16, 23 GeV/c).
[6](a) P. Borzatta *et al.*, Nuovo Cimento A15, 45 (1973) (11.2 GeV/c); (b) D. Brick *et al.*, Phys. Rev. Lett. 31, 488 (1973) (15 GeV/c); (c) P. Bosetti *et al.*, Nucl. Phys. B81, 61 (1974) (16 GeV/c).
[7]D. Fong *et al.*, Phys. Lett. 53B, 290 (1974).
[8]D. Fong *et al.*, Nucl. Phys. B102, 386 (1976).
[9]D. Ljung, Proportional Hybrid System Consortium Newsnote No. 31, Yale Univ., 1974 (unpublished).
[10]J. D. Jackson, Nuovo Cimento 34, 1644 (1964).
[11]The form used was

$$\sigma(M) = \sigma B \frac{M}{q} \frac{\Gamma}{(M^2 - M_0^2)^2 + M_0^2\Gamma^2} + A_0B_0 + A_1B_1M + A_2B_2M^2 + A_3B_3M^3,$$

where $\Gamma = \Gamma_0(q/q_0)^3 p/\rho_0$ is the width of the Δ, $\sigma(M)$ is the cross section at mass M of the $p\pi^+$ combination, $M_0 = 1228$ MeV is the central value of the Δ mass, q is the momentum in the Δ rest frame of one of the decay products,

$\Gamma_0 = 123$ MeV,

$\rho = 1/(2.2 m_\pi^2 + q^2)$,

ρ_0 and q_0 are the values of ρ and q at $M = M_0$. The B's are normalization factors; each term has the value 1 when integrated over the mass range used in the fit. Thus, σ is the cross section for Δ production within the mass range used in the fit, and $A_0 + A_1 + A_2 + A_3$ is the total cross section underneath the Δ signal in the mass range used. The area of the Breit-Wigner term outside of the mass range used was added to the σ from the fit for all cross sections given in this paper.

In some cases the higher-order mass terms were set to 0 to get reasonable fits, i. e., fits having χ^2 per degree of freedom near or less than 1.
[12]M. Bishari, Phys. Lett. 38B, 510 (1972).
[13]E. Gotsman, Phys. Rev. D 9, 1575 (1974).
[14]D. Fong *et al.*, Nuovo Cimento 34A, 659 (1976).
[15](a) E. W. Anderson *et al.*, Phys. Rev. Lett. 25, 699 (1970); (b) J. W. Chapman *et al.*, *ibid.* 32, 257 (1974).
[16]J. Friedman, Lawrence Radiation Laboratory Group A Programming Note No. P-189, 1971 (unpublished).
[17]N. N. Biswas *et al.*, Phys. Rev. D 16, 2090 (1977).
[18](a) D. Fong *et al.*, Phys. Lett. 61B, 99 (1976); (b) V. P. Kenney *et al.*, Notre Dame report, 1975 (unpublished); (c) Y. Eisenberg *et al.*, Phys. Rev. Lett. 38, 108 (1977); (d) T. Ludlum *et al.*, Phys. Lett. 48B, 449 (1974).
[19]D. Fong *et al.*, Nucl. Phys. B104, 32 (1976).
[20]G. Berlad *et al.*, Nucl. Phys. B103, 12 (1976), and references therein.
[21]R. T. Deck, Phys. Rev. Lett. 13, 169 (1964).
[22]E. L. Berger, Phys. Rev. 179, 1567 (1969).
[23](a) I. Ohba and A. Nakamura, Prog. Theor. Phys. 53, 1768 (1975); (b) 54, 1235 (1975).